Desalination 279 (2011) 75–85

Contents lists available at ScienceDirect

Desalination

journal homepage: www.elsevier.com/locate/desal

# Synthesis, structural characterization and Pb(II) adsorption behavior of K- and H-birnessite samples

E. Eren *, H. Gumus, A. Sarihan

*University of Bilecik, Faculty of Science and Arts, Department of Chemistry, 11210, Bilecik, Turkey*

ARTICLE INFO

*Article history:*
Received 23 March 2011
Received in revised form 24 May 2011
Accepted 25 May 2011

*Keywords:*
Birnessite
$MnO_2$
Ion-exchanged birnessite
Adsorption
Pb(II)

ABSTRACT

This paper presents the synthesis, structural characterization and Pb(II) adsorption behavior of K-birnessite and H-birnessite samples. Changes in the surfaces and structure of birnessite samples were characterized by means of infrared spectroscopy (IR), $N_2$ gas adsorption and thermal analysis (TG–DTA) techniques. Adsorption of Pb(II) by samples was investigated as a function of the initial Pb(II) concentration, solution pH, ionic strength, temperature and inorganic ligand ($NO_3^-$, $Cl^-$). The Langmuir monolayer adsorption capacities of K-birnessite and H-birnessite samples in 0.1 M $NaNO_3$ solution at 298 K were estimated as 164.30 and 133.17 mg/g, respectively. Thermodynamic parameters such as change in free energy ($\Delta G$), enthalpy ($\Delta H$) and entropy ($\Delta S$) were evaluated for K-birnessite and H-birnessite to be −22.43 kJ/mol (at 298 K), 23.90 kJ/mol, 155 J/mol K, and −18.50 kJ/mol (at 298 K), 10.57 kJ/mol, 98 J/mol K, respectively.



## 1. Introduction

There are increasing interests in layer-structure materials due to their potential applications in adsorption, catalysis, ion-sieves, and rechargeable batteries [1–4]. Birnessite is a layer-structure manganese oxide with edge-sharing $MnO_6$ octahedra, and has been a subject of intensive investigations due to its ion exchange [5], sorption [6], and redox properties [7,8]. $MnO_6$ layers of birnessite comprise edge-sharing $Mn(IV)O_6$ octahedra, $Mn(III)O_6$ octahedra and cation vacancies [6,9,10]. The vacancies in the structure of birnessite commonly account for the negatively charged layer partially causing adsorption of heavy metals and other pollutants in contaminated water systems and soils.

Adsorption of metal ions by birnessites in aqueous phases is a critical process for the environmental application of birnessites in water treatment as well as for the environmental assessment of physicochemical behaviors of metal ions on birnessites. Recent studies indicated that the structure and surface properties of birnessites strongly depend on chemical composition and synthesis procedures [11,12]. The comparison of adsorption properties for different birnessites and the relevance with their structures is essential for the understanding of their behaviors due to their easily changeable valent states and finely crystalline or poorly ordered forms. However, the investigation about the effect of birnessite structure on the adsorptions of heavy metal ions is still scarce.

The objectives of this work are: (1) to study the adsorption of Pb(II) on birnessites under various common conditions such as pH, ionic strength, inorganic ligands ($NO_3^-$ and $Cl^-$) and temperature by using batch technique; (2) to determine the thermodynamic parameters such as change in free energy ($\Delta G$), enthalpy ($\Delta H$) and entropy ($\Delta S$) of Pb(II) adsorption on birnessites; (3) to characterize the used birnessite samples by infrared spectroscopy (IR), BET and thermal analysis (TG–DTA) techniques; and (4) to presume the adsorption mechanism of Pb(II) on birnessites.

## 2. Experimental

### 2.1. Materials

All reagents, such as NaCl, $NaNO_3$, $HNO_3$, NaOH, $Pb(NO_3)_2$ and $Mn(NO_3)_2.9H_2O$ were all of analytical grade and all solutions were prepared with double distilled water. All reagents used in this work were purchased from Sigma-Aldrich. A solution of 1.0 mM Pb(II) was prepared from $Pb(NO_3)_2$ by dissolution in deionised water. The stock solution was diluted to prepare a working solution.

K-birnessite was prepared according to the redox method described in [13]. 2.85 g $Mn(NO_3)_2$ was dissolved in 450 $cm^3$ distilled water. The 100 $cm^3$ of a solution containing 1.1 g $KMnO_4$ and 0.8 g KOH was added from a fast-dripping burette. A dark Brown to black precipitate was formed immediately and the solution was stirred continuously for 1 h. After stirring, the ssupension was settled for 30 min. Then the excess supernatant was removed and the concentrated suspension was centrifuged and washed several times with distilled water until the supernatatnt conductivity was below $1\times10^{-4}$ M $KNO_3$. The K-birnessite was treated with a 1 M $HNO_3$ solution for 1 day

* Corresponding author. Tel.: +90 228 2160101; fax: +90 228 2160287.
*E-mail address:* erdal.eren@bilecik.edu.tr (E. Eren).

0011-9164/$ – see front matter © 2011 Elsevier B.V. All rights reserved.
doi:10.1016/j.desal.2011.05.058

at room temperature, and then washed with distilled water, and dried at 70 °C, which was designated as H-birnessite.

Infrared (IR) spectra of the birnessite samples were recorded in the region 4000 to 450 $cm^{-1}$ on a a Spectrum-100 FTIR spectrometer. The thermal gravimetric (TG) and differential thermal analyses (DTA) curves were obtained using a PRIS Diamond TG/DTG apparatus in a static air atmosphere (heating rate: 10 °C $min^{-1}$, platinum crucibles, mass ~10 mg and temperature range: 30–1000 °C). A Tri Star 3000 (Micromeritics, USA) surface analyzer was also used to measure the nitrogen adsorption isotherm at 77 K in the range of relative pressure $10^{-6}$ to 1. Before measurement, the sample was degassed at 300 °C for 2 h. The surface areas were calculated by the BET (Brunauer–Emmett–Teller) method.

### 2.2. Adsorption dependence on Pb(II) concentration

The adsorption of Pb(II) by birnessite samples was performed by a batch equilibrium technique at room temperature. Briefly, 0.050 g of birnessite sample and 20 mL of $Pb(NO_3)_2$ solution were added in 50 mL polypropylene centrifuge tubes. In the present work, adsorption could not be carried out beyond pH 6.0 due to precipitation of $Pb(OH)_2$ and therefore, the experiments were done in the pH range 3.0–5.5. The results reveal that adsorption increases with the increase in pH from 3.0 to 5.5 and the maximum adsorption is at pH 5.5, but we chose pH 5.0 to avoid hydrolysis of Pb(II). Ionic strength controlled at 0.1 M $KNO_3$ and the pH of the system was maintained at 5.0. The initial Pb(II) concentrations varied from 0.01 to 1.0 mM. A 24-h contacting period was found to be sufficient to achieve equilibrium. All the measurements were made in duplicate. For each sample, an experiment without adsorbent was performed to test possible adsorption and/or precipitation of metals onto the container walls. Preliminary experiments showed that metal losses due to the adsorption onto the container walls and to the filter paper were negligible. The adsorption isotherm experiments were repeated in triplicate and the average values were reported. Adsorbed Pb(II) was calculated from the difference between the Pb(II) initially added to the system and that remaining in the solution after equilibration by a Unicam 929 model flame atomic absorption spectrophotometer. The dilutions induced by the pH controls were considered while computing the amount of Pb(II) adsorbed.

### 2.3. Effect of ionic strength, pH, inorganic ligand and temperature

Adsorption experiments were carried out in polyethylene test tubes at $23 \pm 2$ °C by using the batch technique. The reaction mixture consisted of a total 50 mL containing 1 g/L adsorbent and the desired concentration of Pb(II) ions. A solution of 1.0 mM Pb(II) was prepared from $Pb(NO_3)_2$ by dissolving in deionisied water. The stock was diluted to prepare a working solution of 0.5 mM Pb(II). The ionic strengths of 0.01, 0.05 and 0.1 M $NaNO_3$ were used to test their effects on Pb(II) adsorbed by K-birnessite and H-birnessite at various initial Pb(II) concentrations. Solution pH was adjusted with 0.1 M $HNO_3$ or 0.1 M NaOH, such that the equilibrium solutions had pH values ranging from 3.0 to 5.5. Preliminary kinetic studies indicated that Pb(II) adsorption was characterized by a rapid initial adsorption (within 1 h) followed by a much slower, continuous uptake. A 24-h contacting period was found to be sufficient to achieve equilibrium. The separation of the liquid from the solid phase was achieved by centrifugation at 4500 rpm for 20 min. The presence of co-ions in solution can affect the adsorption of metal ions onto a charged surface. In this study, the effect of co-ions in solution on adsorption capacity was also investigated. NaCl was chosen and added to the Pb(II) solutions at concentration of 0.01 M. Pb(II) adsorption in the presence of $Cl^-$ was performed by equilibrating 0.05 g of birnessite sample in 20 mL of 0.25 M $NaNO_3$ background electrolyte, 10 mL of Pb(II) working solution, and 20 mL of a NaCl working solution (achieving 0.01 M $Cl^-$) in 50-mL polyethylene test tubes. These experiments were performed in duplicate. The temperature was varied from 298 K to 318 K at a constant pH of 5.0. For these experiments, 124.2 and 41.4 mg/L Pb (II) solutions were employed for 1 g/L of K-birnessite and H-birnessite samples, respectively.

### 2.4. Desorption studies

In this experiment, desorption of Pb(II) from Pb-loaded birnessite samples was performed using $HNO_3$ solution at different concentrations. Pb-loaded birnessite was exposed to 50 mL solution of different $HNO_3$ concentrations (0,001, 0,005, 0,01 and 0,1 M $HNO_3$) in a batch experimental study at 298 K for 2 h. The supernatant was decanted for Pb(II) concentration measurement. Also, desorption experiments were performed using 0.1 M $HNO_3$ in a batch experimental study. The Pb(II)-loaded K-birnessite and H-birnessite were washed with deionised water, respectively, to remove any unadsorbed Pb(II). The K-birnessite and H-birnessite were then re-suspended in 50 mL of 0.1 M $HNO_3$ following the same equilibrium condition for the adsorption process. The solution mixture was filtered and the adsorbent washed several times with distilled water in order to remove excess acid. All experiments were carried out in triplicate with the mean of the results reported.

### 2.5. Data processing

The adsorption percentage of Pb(II) was calculated by the difference of the initial and final concentration using the following equation:

$$R = \frac{(C_0 - C_e)}{C_0} \times 100 \quad (1)$$

where $C_0$ is the initial concentration of Pb(II) solution (mg/L), $C_e$ the equilibrium concentration of the Pb(II) solution (mg/L), R is the adsorbed percentage of Pb(II).

The equilibrium data have been analyzed using the Langmuir and Freundlich isotherms and the characteristic parameters for each isotherm have been determined [14,15]. The data conform to the linear form of the Langmuir model [14] (Eq. (2)) expressed as follows:

$$C_e / q_e = C_e / q_m + 1 / K_L q_m \quad (2)$$

where $C_e$ is the equilibrium concentration of Pb(II) (mg/L) and $q_e$ is the amount of the $Pb^{2+}$ adsorbed (mg) per unit of birnessite (g). $q_m$ and $K_L$ are the Langmuir constants related to the adsorption capacity (mg/g) and the equilibrium constant (L/g), respectively.

The adsorption equilibrium data was also applied to the Freundlich model [15] (Eq. (3)) given as folows:

$$\log q_e = \log K_F + (1/n)\log C_e \quad (3)$$

where $K_F$ and n are the Freundlich constants related to adsorption capacity and adsorption intensity, respectively. The Freundlich parameters ($K_F$ and n) indicate whether the nature of adsorption is either favorable or unfavorable.

The thermodynamic parameters of the adsorption process can be determined from the experimental data as described before [16]. The amount of Pb(II) ions adsorbed at equilibrium at different temperatures (298-318 K) have been examined to obtain the thermodynamic parameters for the adsorption system.

$$\ln K_d = \Delta S / R - \Delta H / RT \quad (4)$$

$$\Delta G = \Delta H - T\Delta S \quad (5)$$

$$K_d = q_e / C_e \quad (6)$$

where $K_d$ is the distribution coefficient for the adsorption, ΔS, ΔH and ΔG are the changes of entropy, enthalpy and Gibbs energy, T (K) is the temperature, R (J $mol^{-1}$ $K^{-1}$) is the gas constant. The values of ΔH and ΔS were determined from the slopes and intercepts of plots of ln $K_d$ vs. 1/T.

The desorption of Pb(II) from the solid phase was calculated as follows:

$$Pb(II)\ desorbed(\%) = \frac{C_d}{C_a} \times 100 \quad (7)$$

where $C_d$ and Ca are the amount of Pb(II) released into the aqueous solution and the amount of Pb(II) adsorbed onto birnessite (mg/L), respectively.

## 3. Results and discussion

### 3.1. Material characterization

Fig. 1a,b shows the infrared spectra (IR) of the K-birnessite and H-birnessite samples between 4000 and 450 $cm^{-1}$. Fig. 1a shows the IR spectrum of the K-birnessite sample. The broad peak at 3412 $cm^{-1}$ is due to stretching vibrations of is interlayer hydrates and some hydroxyl groups not from hydrates but those directly bound to the interlayer metal ions [17]. The peak at 1600 $cm^{-1}$ is assigned to the bending vibration of $H_2O$ and structural OH groups, which implies that hydroxyl groups exist in the K-birnessite.

Fig. 1b shows the IR spectrum of the H-birnessite sample. Several absorption bands were observed at 3391, 1633, 1384, 1024, 823, 722, 570 and 520 $cm^{-1}$, respectively. The 3391 $cm^{-1}$ band should be attributed to stretching vibrations of the O–H group of water molecules and the lattice O–H groups or $H_3O^+$ which are formed by $M^+/H^+$ ion exchange reactions occurring in the acid-treatment process, and the 1633 $cm^{-1}$ band are normally attributed to O-H bending vibrations combined with Mn atoms. Some variations of IR spectra are easily observed. Although bands in the region between 400 and 800 $cm^{-1}$ could be assigned to Mn–O lattice vibration [18–21], the position and intensity of these bands show some changes between K-birnessite and H-birnessite. For K-birnessite sample, two strong IR bands could be observed around 513 and 602 $cm^{-31}$, in good agreement with the IR characteristic bands of birnessites [18–21].

In compare with the IR spectrum of K-birnessite sample, some obvious changes can be observed for H-birnessite. At first, the intensities of Mn–O lattice vibration bands become weak and are shifted to different wave numbers. The bands around 476 and 520 $cm^{-1}$ corresponding to birnessite structure are observed, suggesting the maintenance of the structure [18–20]. Second, a new adsorption band around 722 $cm^{-1}$ is observed, which could be assigned to the characteristic adsorbent of manganese oxides with tunnel structure [21].

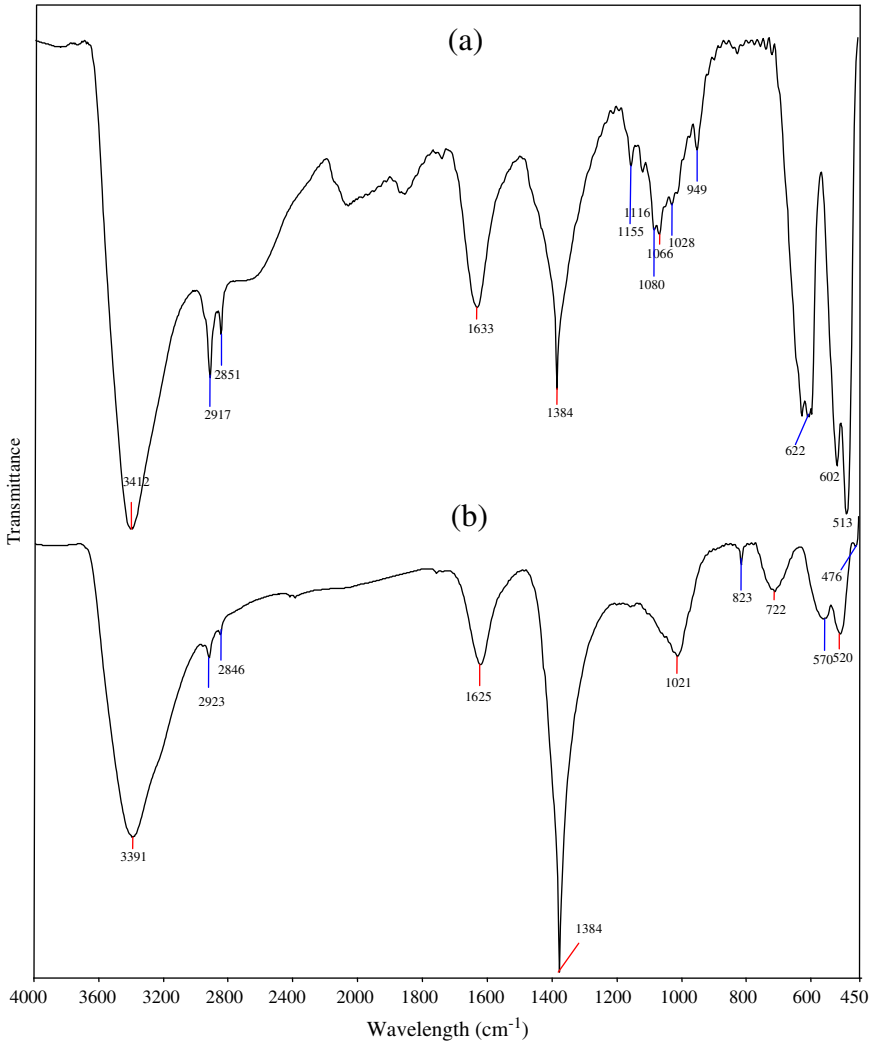


**Fig. 1.** IR spectra of the K-birnessite (a) and H-birnessite (b) samples.

Detailed analysis of IR spectra in the region between 4000 and 400 $cm^{-1}$ can be used to discern the location of Pb(II) cations. The structural modifications of surface due to the adsorbed Pb(II) cations influenced the fundamental vibrations of OH and Mn–O groups (Fig. 2a,b). The stretching OH band for K-birnessite/Pb(II) was moved to 3318 $cm^{-1}$, broadened and decreased in intensity. The absorbance at 1633 $cm^{-1}$ dissapeared after lead adsorption process onto K-birnessite sample, suggesting the removing of the absorbed water with the replacement of the introduced lead species. The IR spectrum of K-birnessite/Pb(II) has shown that Pb(II) ions locate into the birnessite lattice, and also affects Mn–O vibrations in the 1200–450 $cm^{-1}$ region (Fig. 2a). For the K-birnessite/Pb(II) sample, the bands at 1080, 1066 and 1028 $cm^{-1}$ were replaced by a broad band at 1062 $cm^{-1}$. But for Pb(II) inserted K-birnessite sample, the four medium bands (513, 602, 622 and 630 $cm^{-1}$) changed to two ones (616 and 505 $cm^{-1}$) and a new band around 835 $cm^{-1}$ was observed. The change in the intensities and wavelenghts of the bands in the 1200–450 $cm^{-1}$ region confirm the involvement of the Mn–O bond linkage in the Pb(II) adsorption process. The changes in the intensities of these bands are also linked to Pb(II) adsorption, therefore these bands can be considered as the indicator of Pb(II) adsorption process. Their intensities are connected with the ion-exchange of $K^+$ or $H^+$ cations for lead cations.

As the H-birnessite altered to H-birnessite/Pb(II), changes in the IR absorption bands of the sample were noted at 3391, 1625, 1021, 823, 722, 570, and 520 $cm^{-1}$ (Fig. 2b). In the spectrum of H-birnessite/Pb(II), the stretching OH band disappeared and, moreover, a new band appeared near 3743 $cm^{-1}$. The position of water band shifted from 1625 to 1604 $cm^{-1}$ and the broad band at 1021 $cm^{-1}$ in the H-birnessite also disappeared upon Pb(II) adsorption process. The peak at 823 $cm^{-1}$ disappeared, after lead adsorption onto H-birnessite sample. Also, the position of the Mn–O bond vibration at 722 $cm^{-1}$ remained basically unchanged for the H-birnessite/Pb(II) sample, but some broadening and an increase in intensity of this band vibration was observed. After Pb(II) adsorption process, an increase in wavenumber from 570 and 520 $cm^{-1}$ in the H-birnessite/Pb(II) sample to 593 and 529 $cm^{-1}$ was observed. These suggest that the lead adsorption may have effected on the Mn–O lattice vibration bands.

As shown in Fig. 2a and b, a sharp band at 1384 $cm^{-1}$ is observed for birnessite samples [22]. This band shows that a large amount of $NO_3^-$ is retained in the dried intercalated samples of the present work, despite a thorough washing process applied in present work. Accordingly, the occurrence of $NO_3^-$ reflects that there exist some redundant positive-charged mangane aggregates outside the interlayer space of birnessites, and the $NO_3^-$ anions act as counterions to neutralize the redundant positive charge present in the interparticles. The presence of $NO_3^-$ in these samples is of academic importance, since $NO_3^-$ could be utilized as an exchangeable site for other anions, and the content of $NO_3^-$ could be controlled to some extent by adjusting the experimental conditions.

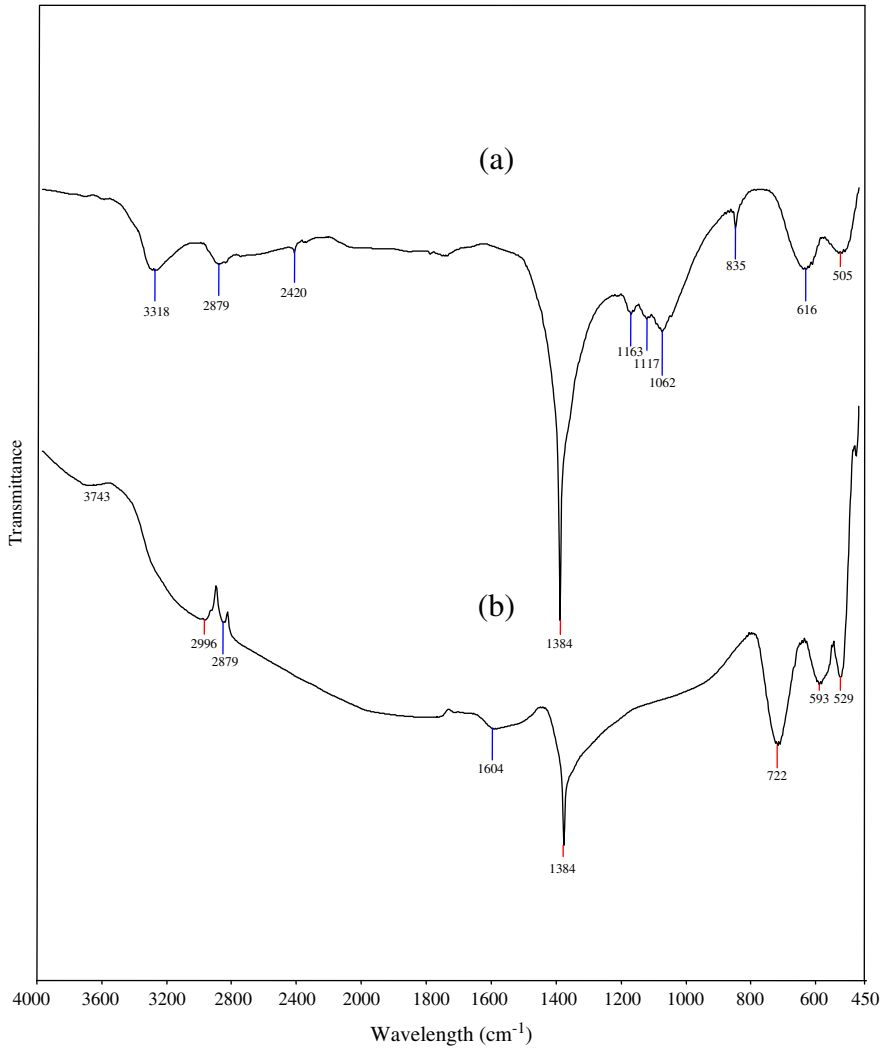


**Fig. 2.** IR spectra of the K-birnessite/Pb(II) (a) and H-birnessite/Pb(II) (b) samples.

The thermal stability of K-birnessite and H-birnessite samples was investigated by TG and DTA (Fig. 3a,b). The curve related to the K-birnessite exhibited mass losses by 10.48 and 7.18% in temperature ranges 20–200 and 200–1000 °C, respectively (Fig. 3a). The two endothermic peaks in the DTA curve of K-birnessite in the range of 20–200 °C denote the release of different water species coordinated to the interlayer cations and surface humidity. Therefore, the endothermic peak at 73 °C can be assigned to the evaporation of adsorbed water, and the endothermic peak at 165 °C to the dehydration of the cation-coordinated water from the interlayer space. The DTA curve had a broad endothermic peak at 486 °C. This is probably due to the departure of oxygen corresponding to its reduction into $Mn_2O_3$ [23–26]. The exothermic peak at 526 °C corresponds to a structural transformation reaction from the layered structure of K-birnessite to the tunnel structure [27]. The TG curve gradually increased with no distinct endothermic/exothermic peak in the range of temperature between 519 and 750 °C. The K-birnessite structure completely collapsed at 924 °C [28]. Therefore, the endothermic peak at about 884 °C in DTA curve corresponds to the transformation of K-birnessite and Mn2O3 to Mn3O4. Thus, the TG curve between 312 and 848 °C indicates that both the manganese oxide phases, i.e. K-birnessite and $Mn_2O_3$ coexists with a very slow transition towards $Mn_3O_4$.

The curve relating to the H-birnessite sample exhibited mass loss 16.6% at 20–200 °C and 17.1% at 200–1000 °C. This material has endothermic peaks around 109, 499, 580, 870, and 943 °C, each corresponding to a weight loss, and an exothermic peak around 553 °C were detected, as shown in Fig. 3b. The endothermic peak at 109 °C corresponds to the evaporation of (surface) adsorbed water in the H- birnessite. The endothermic peaks around 499, 870, and 943 °C can be assigned to the partial transformation of H-birnessite phase to $Mn_2O_3$ (release of oxygen from the H-birnessite phase), transformation of a $Mn_2O_3$ phase to $Mn_3O_4$ phase (associated with the release of oxygen) and collapsing of the H- birnessite, respectively. As shown in Fig. 3b, TG curve for H-birnessite shows approximately smooth mass loss in the range of temperature between 580 and 818 °C. This indicates that the structure of the H-birnessite sample is stable. Also, the stable range of thermogram between 580 and 818 °C indicates that both the manganese oxide phases, i.e. $MnO_2$ and $Mn_3O_4$ coexists with a very slow transition towards $Mn_3O_4$. The endothermic peak at 870 °C for H-birnessite is assigned to the phase transformation of

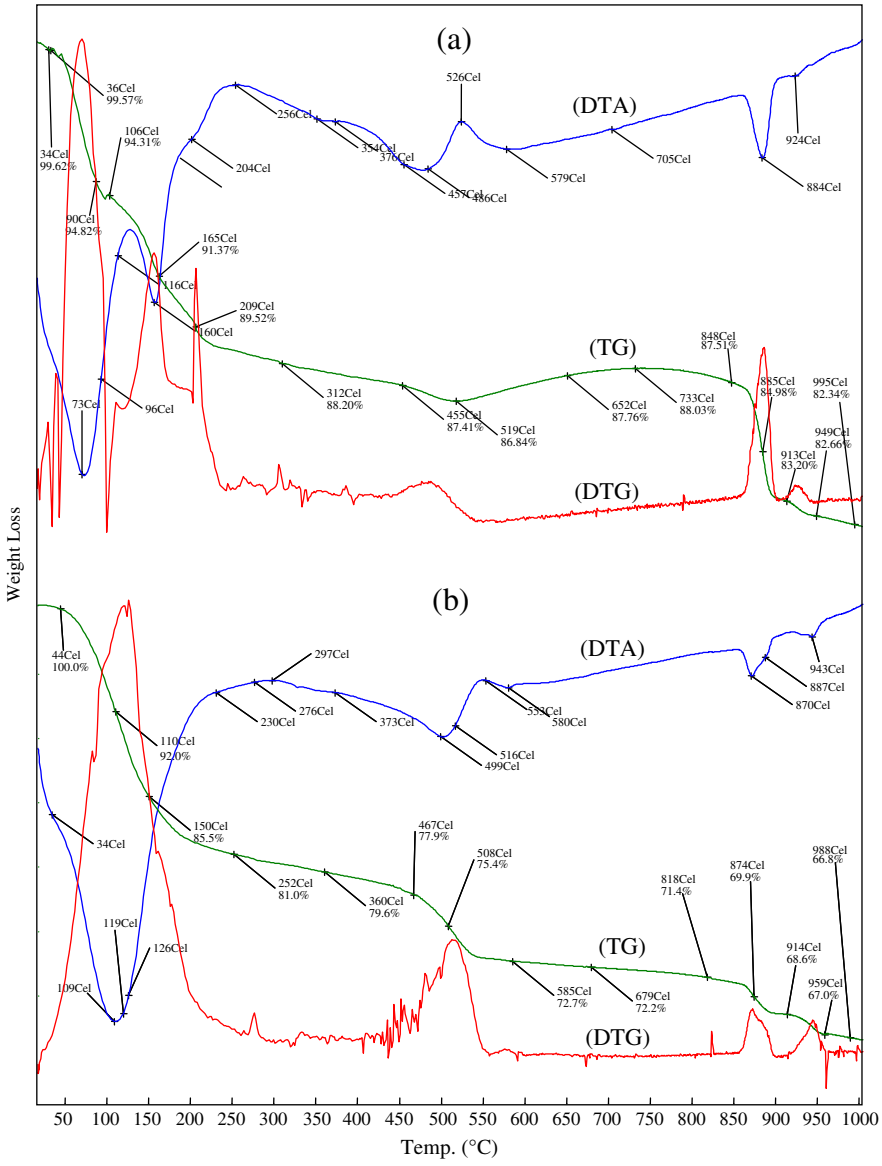


**Fig. 3.** Thermal analysis curves of the K-birnessite (a) and H-birnessite (b) samples.

$Mn_2O_3$ to $Mn_3O_4$. In H-birnessite sample, the lower temperature for $Mn_3O_4$ formation may be attributed to the latice irregularities and dislocations within the crystals.

The dehydration of K-birnessite/Pb(II) occurs with a mass loss of 6.40% whereas this same process happens with a mass loss of 10.48% for K-birnessite in the temperature range of 30–200 °C. The dehydroxilation of K-birnessite/Pb(II) occurs with a mass loss of 3.3% in the temperature range of 200–250 °C as a single-step process which gives rise to an endothermic maximum at 230 °C (Fig. 4a) The same process becomes in one stage in the range of 200–250 °C; a shoulder at 204 °C with a mass loss of 0.79% for K-birnessite. For lead adsorbed birnessites DTA curves show an intense endothermic DTA signal at 300 °C. As is known, decomposition of $PbO_2$ to give $Pb_3O_4$ begins at 280 °C and is complete at 400 °C [29,30]. Morachevskii et al. [29] emphasized that all lead oxides that are richer in oxygen than PbO completely decompose into PbO and $O_2$ at temperatures exceeding 600 °C and the only stable oxide at higher temperatures is PbO. The final dehydroxilation stage is accompanied by a peak at 506 °C, a a shallow endotherm at 446 °C. It is noted that in the range of 600–900 °C, no peak has been appeared on DTA curve of K-birnessite/Pb(II) sample. In overall, it was observed that the parent sample (K-birnessitte) was stable up to higher temperatures rather than the lead-adsorbed K-birnessite sample. A possible explanation is that performing lead-adsorption results in almost framework distortion. It is known that such distortion and the loss of crystallinity occur to a far greater extent in the sample including bigger cations, which make them more prone to thermal collapse than the parent sample. This is in agreement with our results as lead is a bigger cation than potasium.

TG–DTA analysis for H-birnessite/Pb(II) is reported in Fig. 4b as an example of thermal stability characterization. The evolution of adsorbed and cation-coordinated water species from H-birnessite/Pb(II) is represented by an endothermic peak at 73 °C and a shoulder at 177 °C, respectively, in the range of 30–200 °C with a mass loss by 6.1%. The amount of adsorbed water removed for H-birnessite/Pb(II) (4.1%) is lower than that of K-birnessite/Pb(II) (8%). This result indicated that the large size of lead cation results in the reduction of the micropore volume accessible to water molecules and consequently, decreasing the packing efficiency of water molecules in the micropore H-birnessite cavities. The mass losses by 0.65% determined which are accompanied by the endothermic peaks centred at 238 and 267 °C in the range of

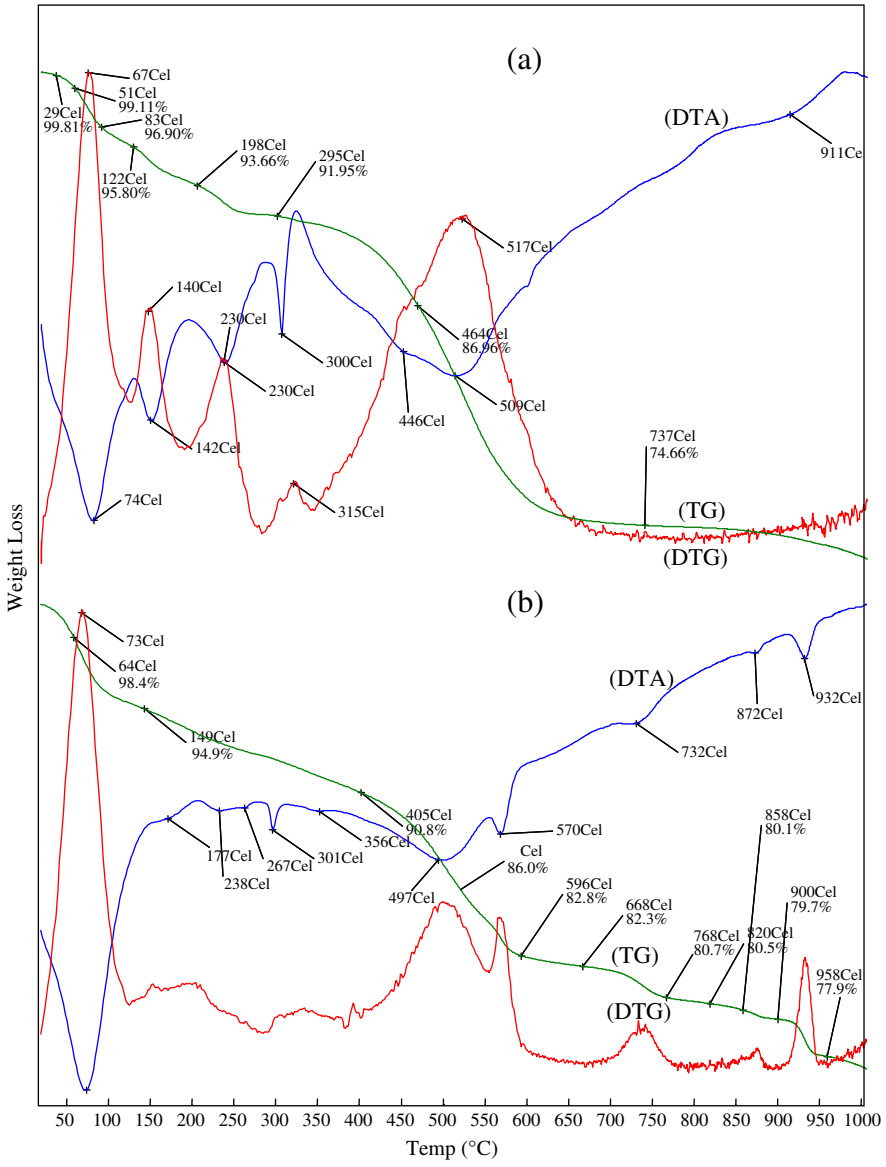


**Fig. 4.** Thermal analysis curves of the K-birnessite/Pb(II) (a) and H-birnessite/Pb(II) (b) samples.

200–270 °C, respectively (Fig. 4a,b) are attributed to the hydration shells around lead cations as a 2-step dehydroxilation process, respectively. Also, this results showed that lead promoted the dissociation of water and the formation of hydroxyl groups. Thermal analyses of lead containing H-birnessite show a similar behaviour to that of parent sample in the range of 500–1000 °C, but with lower weight losses, being 9.7% for H-birnessite sample and 8.8% for H-birnessite/Pb(II) sample. The changes in the high temperature effects, ca. 872 °C, are also remarkable. At this temperature, the phase transformation of $Mn_2O_3$ to $Mn_3O_4$ of the birnessite structure happens. This effect is observed at nearly same temperature and becomes less intense in the presence of lead cation.

The characteristics of the porous structure, including the BET surface area, the pore volume, and the pore size, obtained from the conventional nitrogen isotherm analysis are presented in Table 1. The H ion-exchange process leads to a simultaneous pore widening and an increase in both the pore volume. As shown in Table 1, H-birnessite has the higher surface area and total pore volume and the lower micropore volume than K-birnessite. $HNO_3$ treatment increases K-birnessite's surface area and total pore volume, which not comes from the increase in micropores. The potassium ions may screen out some of the birnessite surface roughness, which becomes inaccessible for the nitrogen molecules and then decreases the BET surface area. Another possibility heading to the reduction of the BET surface area comes from the fact that potasium cation may clog some of the smaller pores, i.e., the pore blocking effect occurs.

### 3.2. Adsorption isotherms and parameters

The effect of temperature on the adsorption equilibrium was investigated under isothermal conditions in the temperature range of 298–318 K. The parameters for the isotherms obtained from Figs. 5 to 8 are presented in Table 2. The temperature of solution plays an important role in the whole adsorption processes. The regression coefficients obtained from the Langmuir and Freundlich models are higher than 0.94, suggesting that both the Langmuir and Freundlich models can be employed to describe the adsorption isotherms of K-birnessite and H-birnessite for Pb(II) at the temperature range studied.

The Langmuir monolayer adsorption capacities varied from 164.30 to 189.13 mg/g for K-birnessite, these values varied from 133.17 to 147.42 mg/g for H-birnessite in the range of temperature between 298 and 318 K. The increase of adsorption capacities of K-birnessite and H-birnessite for Pb(II) ions with increase in temperature indicates the endothermic nature of the adsorption processes. It is known that the adsorption process takes place by two consequent processes fast diffusion and slow complexation. The increase in temperature not only increases the rate of diffusion of the Pb(II) ions present in the bulk solution to the birnessite surfaces but also increases the rate of complexation with the functional groups present on the birnessite surfaces. The adsorption constant, $K_L$, also increased from 0.182 to 0.265 L/mg for K-birnessite and that for H-birnessite increased from 0.017 to 0.020 L/mg with increasing temperature from 298 to 318 K. Large values of $K_L$ indicates that the equilibrium is predominantly

**Table 1**
Porous structure parameters of the K-birnessite and H-birnessite samples.

| Sample | $S_{BET}$ ($m^2/g$) | $S_{ext.}$[a] ($m^2/g$) | $S_{mic.}$ ($m^2/g$) | $V_t$ ($cm^3/g$) | $V_{mic.}$ ($cm^3/g$) | $D_p$[b] (nm) |
|---|---|---|---|---|---|---|
| K-birnessite | 34.24 | 28.56 | 5.68 | 0.169 | 0.0027 | 19.79 |
| H-birnessite | 42.44 | 38.79 | 3.46 | 0.210 | 0.0015 | 19.84 |

[a] $S_{ext} = S_{meso.}$
[b] 4V/A by BET.

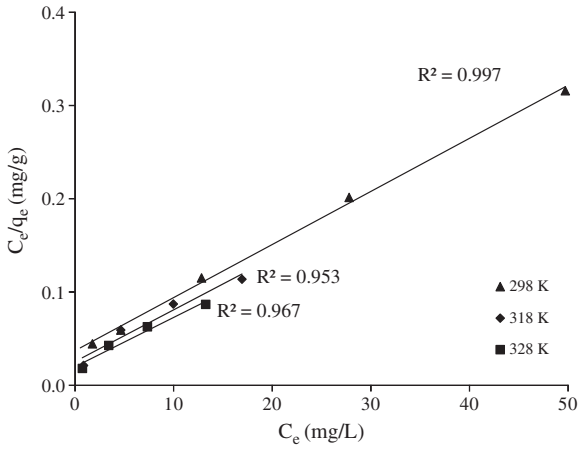


**Fig. 5.** Langmuir isotherm plot for the adsorption of Pb(II) onto K-birnessite sample at different temperatures. Initial pH = 5.0, m = 1 g/L, ionic strength (IS) is 0.1 M $NaNO_3$ (controlled by $NaNO_3$).

driven toward the right, leading to the formation of the adsorbate-adsorbent complex. The value of $K_L$ for H-birnessite is greater than that for K-birnessite. This result indicates that the adsorption of Pb(II) by H-birnessite requests less energy than that of K-birnessite. Moreover, the high value of $K_L$ has been related to specifically adsorbed metal at high energy surfaces with low dissociation constants; while the low value of $K_L$ appears to be related to adsorption at low energy surfaces with high dissociation constants. So, the low $K_L$ value of H-birnessite may indicate that the adsorption of Pb(II) on H-birnessite occurred mainly on specific adsorption positions.

The equilibrium data also fitted to Freundlich equation (Figs. 6 and 8), a fairly satisfactory empirical isotherm can be used for non-ideal adsorption. $K_F$ relates the multilayer adsorption capacity and n intensity of adsorption, which varies with the heterogeneity of the adsorbent [31–33]. A relatively $n << 1$ indicates that adsorption intensity is favorable over the entire range of concentrations studied, while $n > 1$ means that adsorption intensity is favorable at high concentrations but much less at lower concentrations [31,33]. The Freundlich adsorption capacity ($K_F$) for the H-birnessite sample was found to be lower than that for the K-birnessite. In the adsorption systems, the n values are

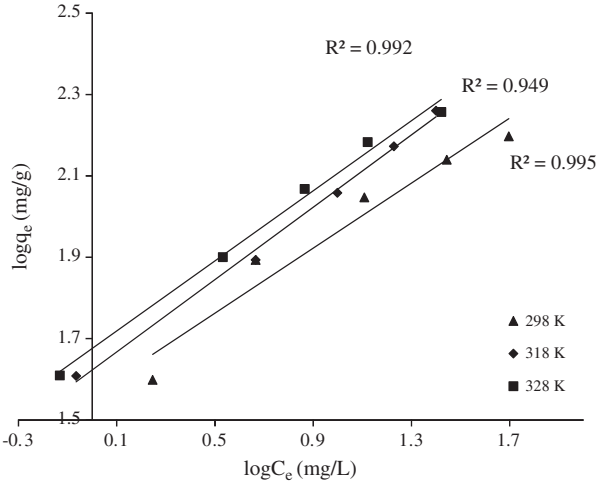


**Fig. 6.** Freundlich isotherm plot for the adsorption of Pb(II) onto K-birnessite sample at different temperatures. Initial pH = 5.0, m = 1 g/L, ionic strenght (IS) is 0.1 M $NaNO_3$ (controlled by $NaNO_3$).

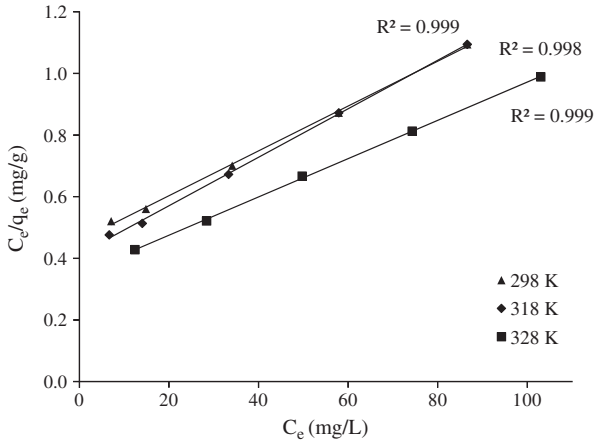


**Fig. 7.** Langmuir isotherm plot for the adsorption of Pb(II) onto H-birnessite sample at different temperatures. Initial pH = 5.0, m = 1 g/L, ionic strenght (IS) is 0.1 M $NaNO_3$ (controlled by $NaNO_3$).

higher than 1 which point out that adsorption intensity is favorable at high concentrations.

The adsorption capacities of the birnessites for the removal of Pb(II) have been compared with those of various adsorbents reported in literature and the values of adsorption capacities have been presented in Table 3. The values are reported in the form of monolayer adsorption capacity. The experimental data of the present investigation are comparable with the reported values [11,34–42].

### 3.3. Effect of ionic strength, pH and inorganic ligand

Adsorption of Pb(II) on birnessite samples in the pH range of 2.0–5.5 is shown in Fig. 9 in 0.01, 0.05 and 0.1 M $NaNO_3$ solutions, respectively. The ionic strength dependence of lead's removal from solution by birnessite samples can be used to distinguish between non-specific and specific adsorption. This might indicate that the influence of the ionic strength on the activity coefficients of lead ions, which limit their transfer to the adsorbent surfaces. Also, the effect of ionic strength on metal adsorption process from aqueous solution is used to distinguish between ion exchange and surface complexation. The strong pH and ionic strength dependent adsorption indicates that adsorption of metal cation is controlled by ion exchange and surface complexation mechanism. Generally, surface complexation is pH dependent, whereas ion exchange is ionic strength dependent.

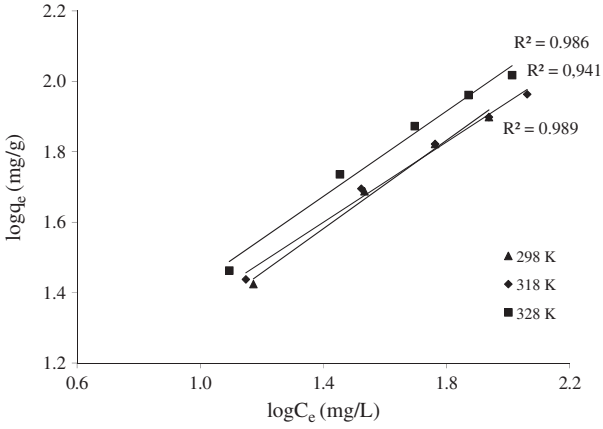


**Fig. 8.** Freundlich isotherm plot for the adsorption of Pb(II) onto H-birnessite sample at different temperatures. Initial pH = 5.0, m = 1 g/L, ionic strenght (IS) is 0.1 M $NaNO_3$ (controlled by $NaNO_3$).

**Table 2**
Langmuir and Freundlich isotherm parameters for the adsorption of Pb(II) onto birnessite samples.

| Sample | T (K) | Langmuir constants | | | Freundlich constants | | |
|---|---|---|---|---|---|---|---|
| | | $q_m$ (mg/g) | $K_L$ (L/mg) | $R^2$ | n | $K_F$ ((mg/g)(L/mg)$^{1/n}$) | $R^2$ |
| K-birnessite | 298 | 164.30 | 0.182 | 0.998 | 2.50 | 36.56 | 0.949 |
| | 308 | 180.35 | 0.218 | 0.954 | 2.25 | 41.96 | 0.996 |
| | 318 | 189.13 | 0.265 | 0.968 | 2.32 | 47.40 | 0.992 |
| H-birnessite | 298 | 133.17 | 0.017 | 0.999 | 1.72 | 5.90 | 0.981 |
| | 308 | 134.93 | 0.018 | 0.998 | 1.75 | 6.34 | 0.991 |
| | 318 | 147.42 | 0.020 | 0.997 | 1.65 | 6.70 | 0.986 |

The adsoption curves for K-birnessite and H-birnessite samples are characterized by one distinct adsorption edge. For example, when the concentration of $NaNO_3$ varied from 0.01 to 0.1 M, the adsorption amount of Pb(II) at pH 5.5 was decreased from 102.0 to 88.5 mg/g for K-birnessite, and 55.0 to 39.0 mg/g for H-birnessite. This may be due to the following two reasons: i — The effect of ionic strength on lead adsorption may be explained by the formation of outer-sphere complexes since $Na^+$ in the background electrolyte could compete with the lead ions adsorbed on the outer-sphere adsorption sites and reduced the adsorption, whereas $Na^+$ would not have competed for the inner-sphere sites [43]. ii — The electrostatic attraction seems to be a significant mechanism, as indicated by the results where at high ionic strength, the increased amount of $NaNO_3$ can help to render the surface of the birnessite samples not easily accessible to Pb(II) ions. According to the electrical diffuse double layer theory, when solid adsorbent is in contact with sorbate species in solution, they are bound to be surrounded by an electrical diffused double layer, the thickness of which is significantly expanded by the presence of electrolyte. Such expansion may be inhibited the approaching between birnessite particles and Pb(II) cations. Due to these reasons, the decreasing amount of adsorbed lead ions with increasing $NaNO_3$ concentration may be explained by the ions at the birnessite surface contributing the adsorption and complexation of Pb(II). From Fig. 9, it can see that the adsorption of Pb(II) on K-birnessite above pH 5.5 is weakly dependent on the ionic strength of the medium. The ionic strength independent adsorption at pH value above 5.5 suggests that inner-sphere complexation/chemical adsorption is the main adsorption mechanism of Pb(II) onto K-birnessite. The ionic strength dependent adsorption indicates that ion exchange or outersphere complexation contributes to Pb(II) adsorption on H-birnessite at pH value above 3.0.

**Table 3**
Adsorption results of Pb(II) ions from the literature by various adsorbents.

| Adsorbent | Adsorption capacity (mg/g) | Ref. no |
|---|---|---|
| Mn oxide minerals | 379.6–21.8 | 11 |
| Birnessites with different average oxidation states | 375.9–108.6 | 34 |
| Low grade manganese ore | 142.85 | 35 |
| Na-birnessite | 117.5 | 36 |
| β-$MnO_2$ | 13.57 | 37 |
| $CeO_2$ nanoparticles | 189 | 38 |
| $Fe_3O_4$ nanoparticles | 83 | 38 |
| $TiO_2$ nanoparticles | 159 | 38 |
| Iron oxide nanoparticles | 36.0 | 39 |
| $Al_2O_3$ | 17.5 | 40 |
| $Al_2O_3$-supported iron oxide (300 K, pH 5) | 28.98 | 41 |
| Diatomite (pH 5, 24 h) | 24.0 | 42 |
| Mn-diatomite (pH 5, 24 h) | 99.0 | 42 |
| K-birnessite (IS = 0.1 M $NaNO_3$) | 164.30 | *In this study* |
| MCB (IS = 0.1 M $NaNO_3$) | 133.17 | *In this study* |

IS: Ionic strength (controlled by $NaNO_3$).

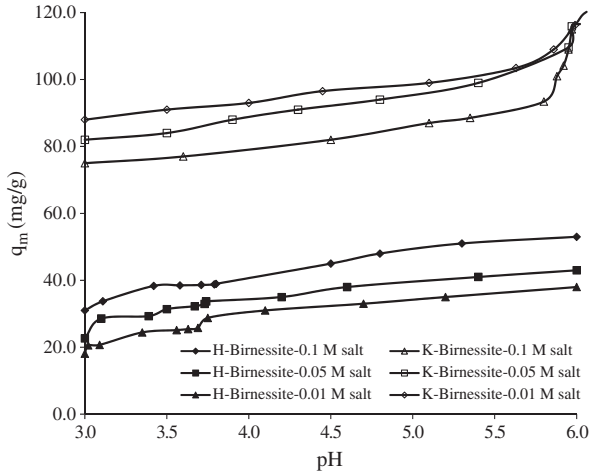


**Fig. 9.** Adsorption of Pb(II) by samples (1 g/L) as function of pH and ionic strength (124.2 and 41.4 mg/L Pb(II) for K-birnessite and H-birnessite, respectively).

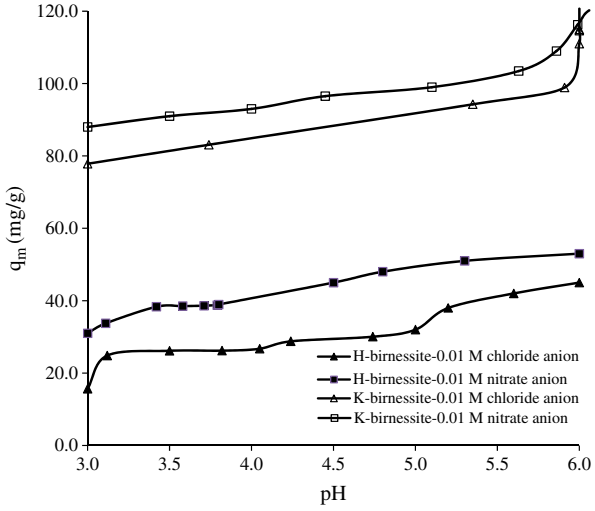


**Fig. 10.** Adsorption of Pb(II) by samples (1 g/L) as function of pH and in the presence of inorganic ligands (124.2 and 41.4 mg/L Pb(II) for K-birnessite and H-birnessite, respectively).

Fig. 10 shows the adsorption curves of Pb(II) on birnessite samples as a function of pH in 0.01 M $NaNO_3$ and NaCl solutions, respectively. The adsorbed Pb(II) in the presence of inorganic ligands may be also attributed to a high specifity of the surfaces for Pb(II) relative to ligands. The adsorption of Pb(II) ions by the birnessite samples was influenced by the presence of $Cl^-$ and $NO_3^-$ (Fig. 10). The amount of adsorbed lead on K-birnessite and H-birnessite samples in the 0.01 M $Cl^-$ system was decreased in the range of pH between 3.0 and 6.0. The results demonstrate that anions affect Pb(II) adsorption on birnessite sample. This phenomenon may be contributed by the facts that: (I) $Cl^-$ and $NO_3^-$ can form soluble complexes with Pb(II) ion in solution (e.g. $PbCl_x^{(2-x)-}$, $Pb(NO_3)_x^{(2-x)-}$) and by that reduce or completely disable sorption at birnessite. (II) $NO_3^-$ ligand forms less stable complex with Pb(II), which results with higher effect at sorption efficacy. (III) Adsorption of $Cl^-$ to birnessite surface is a little easier than $NO_3^-$ and $Cl^-$ adsorption on the surface of birnessite changes the surface properties of the sample and decreases the availability of binding sites for Pb(II).

### 3.4. Thermodynamic studies

ΔG, ΔH and ΔS values were calculated as −22.43 kJ/mol (at 298 K), 23.90 kJ/mol and 155 J/mol K for K-birnessite sample, and −18.50 kJ/mol (at 298 K), 10.57 kJ/mol and 98 J/mol K for H-birnessite sample (Table 4). The negative values for the Gibbs free energy change, ΔG, show that the adsorption process for the two birnessite samples is spontaneous and the degree of spontaneity of the reaction increases with increasing temperature. The increase in adsorption with temperature may be attributed to the increase in the number of active surface sites available for adsorption on the adsorbent and the decrease in the thickness of the boundary layer surrounding the adsorbent with temperature. The positive values of ΔH indicate the endothermic behavior of adsorption reaction. This fact was proved by the increase in the adsorption of Pb(II) with temperature in Section 3.2. The positive values of ΔH suggest that a large amount of heat is consumed to transfer the Pb(II) ions from aqueous into the solid phase. This result may be explain by the following reasons: The higher Pb(II) removal due to increasing temperature may be attributed to intereaction taking place between the adsorption sites of K-birnessite and Pb(II). The exchange of the Pb(II) with $H^+$ need the bond breaking of OH groups on K-birnessite surface, which is an endothermic process. Also, the sorption of Pb(II) require a diffusion process, which is an endothermic process; i.e., the rise of temperature favors Pb(II) transport within the particles of K-birnessite. The positive values of ΔS reflect the affinity of the birnessite samples for Pb(II) and indicate the increased randomness at the solid–solution interface due to the decreases in the hydration of the adsorbing Pb(II) cations. Pb(II) cations must give up a larger share of their hydration water before they could introduce the surface. Such a release of water from Pb(II) cations causes the positive values of ΔS.

Thermodynamic data on Pb (II) ions adsorption on manganese oxides are scarce and the reported values of adsorption thermodynamic parameters have been presented in Table 4. The experimental adsorption thermodynamic data of the present investigation are comparable with reported values.

### 3.5. Desorption of Pb(II)

The result of the desorption test carried on birnessite samples using different $HNO_3$ concentrations is presented in Fig. 11. As seen, the desorption efficiency increased with the increase in $HNO_3$ concentration. No significant desorption was observed in the deionised water;

**Table 4**
Thermodynamic parameters for the adsorption of Pb(II) onto raw and pre-treated manganese oxide samples.

| Sample | ΔH (kJ $mol^{-1}$) | ΔS (J $mol^{-1}$ $K^{-1}$) | ΔG (kJ $mol^{-1}$) | | | Ref. no |
|---|---|---|---|---|---|---|
| | | | 298 K | 303 K | 313 K | |
| β-$MnO_2$ | 10.36 | 124.94 | −17.93 | −19.18 | −20.43 | [37] |
| $MnO_2$ coated carbon nanotubes | 0.0353 | 22.93 | −6.80 | −7.03 | −7.26 | [44] |
| $MnO_2$ coated zeolite | 9.35 | 200 | −50.25 | −52.25 | −54.25 | [45] |
| $MnO_2$ coated sand | 18.2 | 117 | −16.67 | −17.84 | −19.01 | [46] |
| K-birnessite | 23.90 | 155 | −22.43 | −23.99 | −25.54 | *In this study* |
| H-birnessite | 10.57 | 98 | −18.50 | −19.48 | −20.45 | *In this study* |

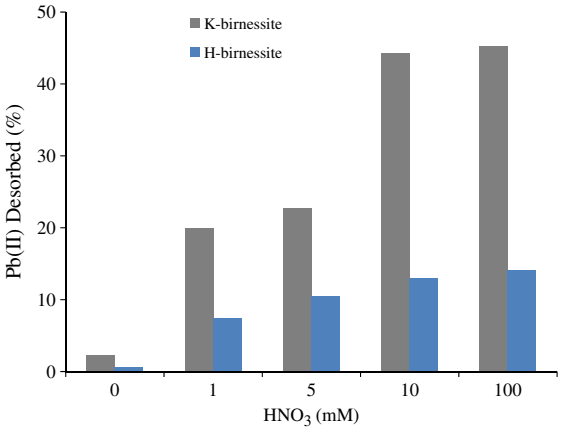


**Fig. 11.** Desorption of Pb(II) from Pb(II)-loaded birnessite samples using different concentrations of $HNO_3$ solution. Adsorbent amount: 1 g/L, contact time: 2 h, T = 298 K.

while almost 45 and 14% desorption for K-birnessite and H-birnessite birnessite samples, respectively, was obtained at 0.1 M $HNO_3$. This suggests that the adsorption of Pb(II) onto birnessite samples is irreversible, and the bonding between the active sites and the adsorbed Pb(II) is strong.

## 4. Conclusions

In the present work, a cheap, readily available and effective adsorbent material has identified birnessite as a potentially attractive adsorbent for the treatment of Pb(II) contaminated aqueous solutions. The adsorption of Pb(II) by birnessite samples was influenced by pH, ionic strength, and the presence of inorganic ligands. The adsorption isotherm studies indicate that the adsorption of Pb(II) follows both the Langmuir and Freundlich isotherms. Three phases, K-birnessite, $Mn_2O_3$ and $Mn_3O_4$, coexisted at below 848 °C. The sharp transition at about 884 °C shows a high transition rate of K-birnessite and $Mn_2O_3$ to higher oxide phase ($Mn_3O_4$). The endothermic peak at 870 °C for H-birnessite is assigned to the phase transformation of $Mn_2O_3$ to $Mn_3O_4$. It is clearly seen that adsorbed lead cation influenced significantly the thermal behavior of the birnessite samples with regard to their dehydration and dehydroxilation capacities. Adsorbed lead cation influenced significantly the thermal behavior of the birnessite samples with regard to their dehydration and dehydroxilation capacities. It was observed that the parent sample (K-birnessitte) was stable up to higher temperatures rather than the lead-adsorbed K-birnessite sample. A possible explanation is that performing lead-adsorption results in almost framework distortion.

## References

[1] W.-Z. Li, Z.-Y. Liu, Y.-L. Che, D. Zhang, Molecular simulation of adsorption and separation of mixtures of short linear alkanes in pillared layered materials at ambient temperature, J. Colloid Interface Sci. 312 (2007) 179–185.
[2] G. Centi, S. Perathoner, Catalysis by layered materials: a review, Micropor. Mesopor. Mat. 107 (2008) 3–15.
[3] Q.-H. Zhang, S.-P. Li, S.-Y. Sun, X.-S. Yin, J.-G. Yu, Lithium selective adsorption on 1-D MnO2 nanostructure ion-sieve, Adv. Powder Technol. 20 (2009) 432–437.
[4] L. Zhang, H. Noguchi, Novel layered Li–Cr–Ti–O cathode materials for lithium rechargeable batteries, Electrochem. Commun. 4 (2002) 560–564.
[5] P. Le Goff, N. Baffier, S. Bach, J.P. Pereira-Ramos, Synthesis, ion exchange and electrochemical properties of lamellar phyllomanganates of the birnessite group, Mater. Res. Bull. 31 (1996) 63–75.
[6] C.L. Peacock, D.M. Sherman, Sorption of Ni by birnessite: equilibrium controls on Ni in seawater, Chem. Geol. 238 (2007) 94–106.
[7] R. Renuka, S. Ramamurthy, An investigation on layered birnessite type manganese oxides for battery applications, J. Power. Sources. 87 (2000) 144–152.
[8] M.A. Rao, G. Iamarino, R. Scelza, F. Russo, L. Gianfreda, Oxidative transformation of aqueous phenolic mixtures by birnessite-mediated catalysis, Sci. Total. Environ. 407 (2008) 438–446.
[9] B. Lanson, V.A. Drits, E. Silvester, A. Manceau, Structure of H-exchanged hexagonal birnessite and its mechanism of formation from Na-rich monoclinic buserite at low pH, Am. Mineral. 85 (2000) 826–838.
[10] A.-C. Gaillot, B. Lanson, V.A. Drits, Structure of birnessite obtained from decomposition of permanganate under soft hydrothermal conditions. 1. Chemical and structural evolution as a function of temperature, Chem. Mater. 17 (2005) 2959–2975.
[11] X.H. Feng, L.M. Zhai, W.F. Tan, F. Liu, J.Z. He, Adsorption and redox reactions of heavy metals on synthesized Mn oxide minerals, Environ. Pollut. 147 (2007) 366–373.
[12] W. Zhao, Q.Q. Wang, F. Liu, G.H. Qiu, W.F. Tan, X.H. Feng, $Pb^{2+}$ adsorption on birnessite affected by Zn2+ and Mn2+ pretreatments, J. Soils Sediments. 10 (2010) 870–878.
[13] X. Li, G. Pan, Y. Qin, T. Hu, Z. Wu, Y. Xie, EXAFS studies on adsorption–desorption reversibility at manganese oxide–water interfaces: II. Reversible adsorption of zinc on δ-MnO2 Original Research Article, J. Colloid Interf. Sci. 271 (2004) 35–40.
[14] I. Langmuir, The adsorption of gases on plane surfaces of glass, mica and platinum, J. Am. Soc. 40 (1918) 1361–1403.
[15] H. Freundlich, Uber die adsorption in losungen, Zeitschrift für Physikalische Chemie (Leipzig) 57 (1906) 385–470.
[16] E. Eren, Removal of copper ions by modified Unye clay, Turkey, J. Hazard. Mater. 159 (2008) 235–244.
[17] U. Bentrup, A. Brückner, M. Richter, R. Fricke, NOx adsorption on $MnO_2$/NaY composite: an in situ FTIR and EPR study, Appl. Catal. B.-Environ. 32 (2001) 229–241.
[18] F. Li, J. Wu, Q. Qin, Z. Li, X. Huang, Facile synthesis of γ-MnOOH micro/nanorods and their conversion to β-$MnO_2$, $Mn_3O_4$, J. Alloy. Compd. 492 (2010) 339–346.
[19] L. Zhang, Z.-H. Liu, X. Tang, J. Wang, K. Ooi, Synthesis and characterization of β-MnO2 single crystals with novel tetragonous morphology, Mater. Res. Bull. 42 (2007) 1432–1439.
[20] Q. Feng, K. Yanagisawa, N. Yamasaki, Synthesis of birnessite-type potassium manganese oxide, J. Mater. Sci. Lett. 16 (1997) 110–112.
[21] L. Kang, M. Zhang, Z.-H. Liu, K. Ooi, IR spectra of manganese oxides with either layered or tunnel structures, Spectrochim Acta. A 67 (2007) 864–869.
[22] E. Eren, H. Gumus, N. Ozbay, Equilibrium and thermodynamic studies of Cu(II) removal by iron oxide modified sepiolite, Desalination 262 (2010) 43–49.
[23] L.I. Liu, Q. Feng, K. Yanagisawa, Y. Wang, Characterization of birnessite-type sodium manganese oxides prepared by hydrothermal reaction process, J. Mater. Sci. Lett. 19 (2000) 2047–2050.
[24] R.M. Cornell, R. Giovanoli, Transformatıon of hausmannite into birnessite, in alkaline media, Clay Clay Miner. 36 (1998) 249–257.
[25] F. Zhou, X. Zhao, C. Yuan, H. Xu, Synthesis of γ-MnOOH nanorods and their isomorphous transformation into β-$MnO_2$ and α-$Mn_2O_3$ nanorods, J. Mater. Sci. 42 (2007) 9978–9982.
[26] O. Prieto, M.D. Arco, V. Rives, Characterisation of K, Na, and Li birnessites prepared by oxidation with H2O2 in a basic medium. Ion exchange properties and study of the calcined products, J. Mater. Sci. 38 (2003) 2815–2824.
[27] L. Liu, Q. Feng, K. Yanagisawa, G. Bignall, T. Hashida, Lithiation reactions of Zn- and Li-birnessites in non-aqueous solutions and their stabilities, J. Mater. Sci. 37 (2002) 1315–1320.
[28] L.-X. Yang, Y.-J. Zhu, G.-F. Cheng, Synthesis of well-crystallized birnessite using ethylene glycol as a reducing reagent, Mater. Res. Bull. 42 (2007) 159–164.
[29] S. Kumar, M. Sharon, S.R. Jawalekar, Preparation of a thin film of Pb3O4 by thermal treatment of $PbO_2$ film, Thin Solid Films 195 (1991) 273–278.
[30] A.G. Morachevskii, Z.I. Vaisgant, V.L. Ugolkov, M.N. Khabachev, E.V. Bochagina, O.A. Kal'ko, Yu.S. Kuznetsova, Reduction in processing of active paste from lead battery scrap, Russ. J. Appl. Chem. 79 (2006) 241–249.
[31] P. Balaz, A. Alacova, J. Briancin, Sensitivity of Freundlich equation constant 1/n for zinc sorption on changes induced in calcite by mechanical activation, Chem. Eng. J. 114 (2005) 115–121.
[32] Y.E. Mouzdahir, A. Elmchaouri, R. Mahboub, A. ElAnssari, A. Gil, S.A. Korili, M.A. Vicente, Interaction of stevensite with $Cd^{2+}$ and $Pb^{2+}$ in aqueous dispersions, Appl. Clay. Sci. 35 (2007) 47–58.
[33] Y.S. Al-Degs, M.I. El-Barghouthi, A.A. Issa, M.A. Khraisheh, G.M. Walker, Sorption of Zn(II), Pb(II), and Co(II) using natural sorbents: equilibrium and kinetic studies, Water Res. 40 (2006) 2645–2658.
[34] W. Zhao, X. Feng, W. Tan, F. Liu, S. Ding, Relation of lead adsorption on birnessites with different average oxidation states of manganese and release of $Mn^{2+}$/$H^+$/$K^+$, J. Environ. Sci. 21 (2009) 520–526.
[35] K. Rout, M. Mohapatra, B.K. Mohapatra, S. Anand, Pb(II), Cd(II) and Zn(II) adsorption on low grade manganese ore, Int. J. Eng. Sci. Technol. 1 (2009) 106–122.
[36] Y. Cho, S. Jang, Y. Kim, S. Komarneni, S. Kim, Uptake of cadmium, copper, and lead by microporous synthetic Na-birnessite, J. Porous. Mater. 18 (2011) 125–131.
[37] D. Zhao, X. Yang, H. Zhang, C. Chen, X. Wang, Effect of environmental conditions on Pb(II) adsorption on β-$MnO_2$, Chem. Eng. J. 164 (2010) 49–55.
[38] S. Recillas, A. García, E. González, E. Casals, V. Puntes, A. Sánchez, X. Font, Use of $CeO_2$, $TiO_2$ and $Fe_3O_4$ nanoparticles for the removal of lead from water: toxicity of nanoparticles and derived compounds, Desalination, doi:10.1016/j.desal.2011.04.036.
[39] N.N. Nassar, Rapid removal and recovery of Pb(II) from wastewater by magnetic nanoadsorbents, J. Hazard. Mater. 184 (2010) 538–546.
[40] S. Yin, Z. Jiang, G. Chang, B. Hu, Simultaneous on-line preconcentration and determination of trace metals in environmental samples by flow injection combined with inductively coupled plasma mass spectrometry using a nanometer-sized alumina packed micro-column, Anal. Chim. Acta. 540 (2005) 333–339.
[41] Y.-H. Huang, C.-L. Hsueh, C.-P. Huang, L.-C. Su, C.-Y. Chen, Adsorption thermodynamic and kinetic studies of Pb(II) removal from water onto a versatile $Al_2O_3$-supported iron oxide, Sep. Purif. Technol. 55 (2007) 23–29.

[42] Y. Al-Degs, M.A.M. Khraisheh, M.F. Tutunji, Sorption of lead ions on diatomite and manganese oxides modified diatomite, Water Res. 35 (2001) 3724–3728.
[43] X. Guo, S. Zhang, X.-Q. Shan, Adsorption of metal ions on lignin, J. Hazard. Mater. 151 (2008) 134–142.
[44] S.-G. Wang, W.-X. Gong, X.-W. Liu, Y.-W. Yao, B.-Y. Gao, Q.-Y. Yue, Removal of lead(II) from aqueous solution by adsorption onto manganese oxide-coated carbon nanotubes, Sep. Purif. Technol. 58 (2007) 17–23.
[45] W. Zou, R. Han, Z. Chen, Z. Jinghua, J. Shi, Kinetic study of adsorption of Cu(II) and Pb(II) from aqueous solutions using manganese oxide coated zeolite in batch mode, Colloid Surf. A. 279 (2006) 238–246.
[46] R. Han, Z. Lu, W. Zou, W. Daotong, J. Shi, Y. Jiujun, Removal of copper(II) and lead(II) from aqueous solution by manganese oxide coated sand: II. Equilibrium study and competitive adsorption, J. Hazard. Mater. 137 (2006) 480–488.